9th ECCOMAS Thematic Conference on the Mechanical Response of Composites
COMPOSITES 2023
G. Catalanotti, H. Petterman and G. Pittaresi (Eds)

IMPACT DAMAGE MODELLING IN COMPOSITE LAMINATES – NUMERICAL IMPLEMENTATION OF A STRAIN RATE DEPENDENT DAMAGE MODEL

Darko Ivančević[1*] and Jakov Ratković[1]

[1] Faculty of Mechanical Engineering and Naval Architecture, University of Zagreb,
Ivana Lučića 5, 10000 Zagreb, Croatia
* divancevic@fsb.hr

Keywords: Composite numerical modelling, Impact damage, Strain rate effects

Summary: *In this work, a numerical methodology for simulation of impact damage in laminated CFRP structures has been developed and implemented into the Abaqus/Explicit software. The methodology is based on the recent insights into the mechanical behaviour of CFRP materials at various strain rates.*

Failure initiation is modelled using the failure theory that was introduced in Coles et al. (2019). This approach has been modified to include the strain rate effects according to work presented in Raimondo et al. (2012) and to account for the mesh objectivity of the damage process in this work. The model has been implemented into Abaqus/Explicit using the user-material subroutine VUMAT and details of the implementation are discussed in the work. The model has been applied to the simulation of two impact simulations demonstrating that the damage modes of the composite plate, as well as damage scope and displacement fields, have been simulated accurately.

The methodology has been previously developed for application in unidirectional composite plates, whereas this work and current research phase focus on woven composites. Additionally, only the in-plane failure modes are currently considered whereas the out-of-plane damage modes will be investigated in the future research.

1. INTRODUCTION

In this work, a numerical methodology is proposed that aims at increasing accuracy in the impact damage modelling in fiber-reinforced structures by the inclusion of the strain rate dependency of the material into the failure modelling process. The strain rate effects in unidirectional Carbon Fiber Reinforced Polymers (CFRP) are extensively documented in the references, e.g. in [1]. In contrast, research focused on woven composite plies is generally less extensively covered in the literature compared to the unidirectional (UD) composites [2].

A common approach in the structural failure modelling of woven composites is the extension of the tensile and compressive criteria for UD composites to the four analogous failure modes of the woven plies – warp and weft tensile and compressive failure. Additionally, the effects caused by the resin-rich zones, that affect the behavior of woven composites, need to be accounted for in these models [3]. An additional property of woven CFRP composites at high strain rates is the pronounced nonlinear behavior in the shear loading modes [4].

In this work, a strain rate dependent constitutive model for woven CFRP composites is presented. The model is still in the development phase and along with the strain rate effects on the strength values, appropriate failure initiation criteria are utilized. Additionally, a progressive damage model is implemented for various failure modes. In order to validate the developed numerical model against existing experimental data, simulations of high velocity impacts on a CFRP rectangular plate have been performed. Further research agenda is proposed, including damage propagation laws and modelling of delamination.

2. METHODOLOGY

The constitutive relations containing the strain rate effects have been implemented in *Abaqus/Explicit* using the VUMAT subroutine written in FORTRAN programming language. The failure initiation theory, introduced in [5], has been selected as the damage initiation model. The model is based on modified Hashin's criteria that have been adjusted to be applicable for woven composite plies and to include the strain rate effects.

2.1. Strain rate dependency

A logarithmic function introduced in [6] has been used in this work to model the strain rate effects on the composite ply strength values. This function is defined as

$$k_{ii}(\dot{\varepsilon}_{ii}) = K_0 + K_1 \cdot \log(|\dot{\varepsilon}_{ii}|) + K_2 \cdot (\log(|\dot{\varepsilon}_{ii}|))^2, \quad (1)$$

where K_0, K_1 and K_2 are the curve fitting parameters used to determine the $k_{ii}(\dot{\varepsilon}_{ii})$ strain rate effect parameter corresponding to strain rate $\dot{\varepsilon}_{ii}$ and strength in the direction ii. The increase of strength values in the elevated strain rate conditions is varying for different loading directions and orientations, leading to the necessity of establishing different curve fitting parameters for separate strengths. This could be observed from Table 1, containing all the fitting parameters used along with the material strength data, taken from [5] for the woven CFRP plies T300 K3/IMP530R and T300 K12/ IMP530R. Due to the lack of extensive and detailed experimental data and for simplicity reasons, values of the K_2 fitting parameters were set to be equal to zero throughout this study. The effects of increased strain rates on the strength values, as defined using eq. (1) and the properties provided in Table 1, is visualized in Figure 1.

Table 1. Quasi-static and dynamic strength data for material systems T300 K3/IMP530R and T300 K12/ IMP530R [5,7], accompanied with strain rate effects fitting parameters K_0 and K_1

Strength [MPa]	Quasi-static	Dynamic	K_0, [-]	K_1, [-]
$X_t(=Y_t)$	520.0	594.2	1.07	0.024
$X_c(=Y_c)$	471.2	849.4	1.40	0.134
Z_t	73.0	107.8	1.24	0.079
Z_c	320.1	348.6	1.04	0.016
$S_{12}(=S_{23}=S_{13})$	100.0	194.5	1.47	0.158

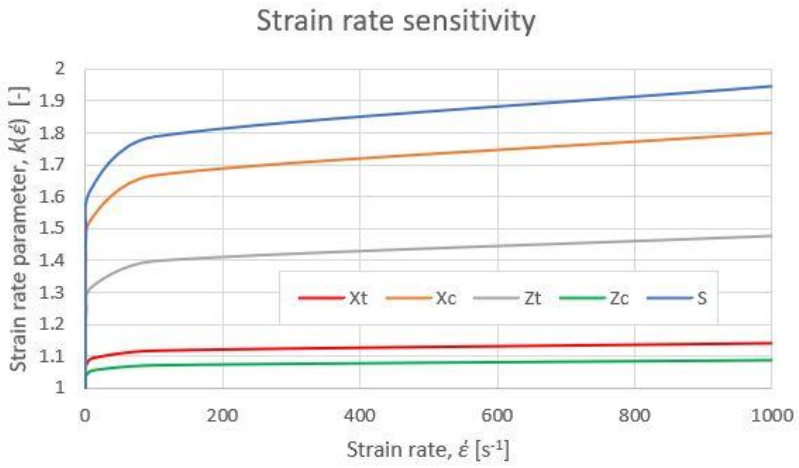

Figure 1. Strain rate parameters $k_{ii}(\dot{\varepsilon}_{ii})$ for different strengths at various strain rates

Failure envelopes in the $\sigma_{11} - \sigma_{22}$, $\sigma_{22} - \sigma_{12}$ and $\sigma_{22} - \sigma_{33}$ stress planes for quasi-static (0.001 s^{-1}), intermediate (1 s^{-1}) and high (1000 s^{-1}) strain rate conditions are shown in the images in Figure 2 a), b) and c), respectively. As shown by these results, the employed fitting parameters and strain rate effect factors are showing a good correlation with the strength data given in Table 1. Currently, shear strength increase due to elevated strain rates is not taken into account in the proposed failure criteria, as the presented model is still in development.

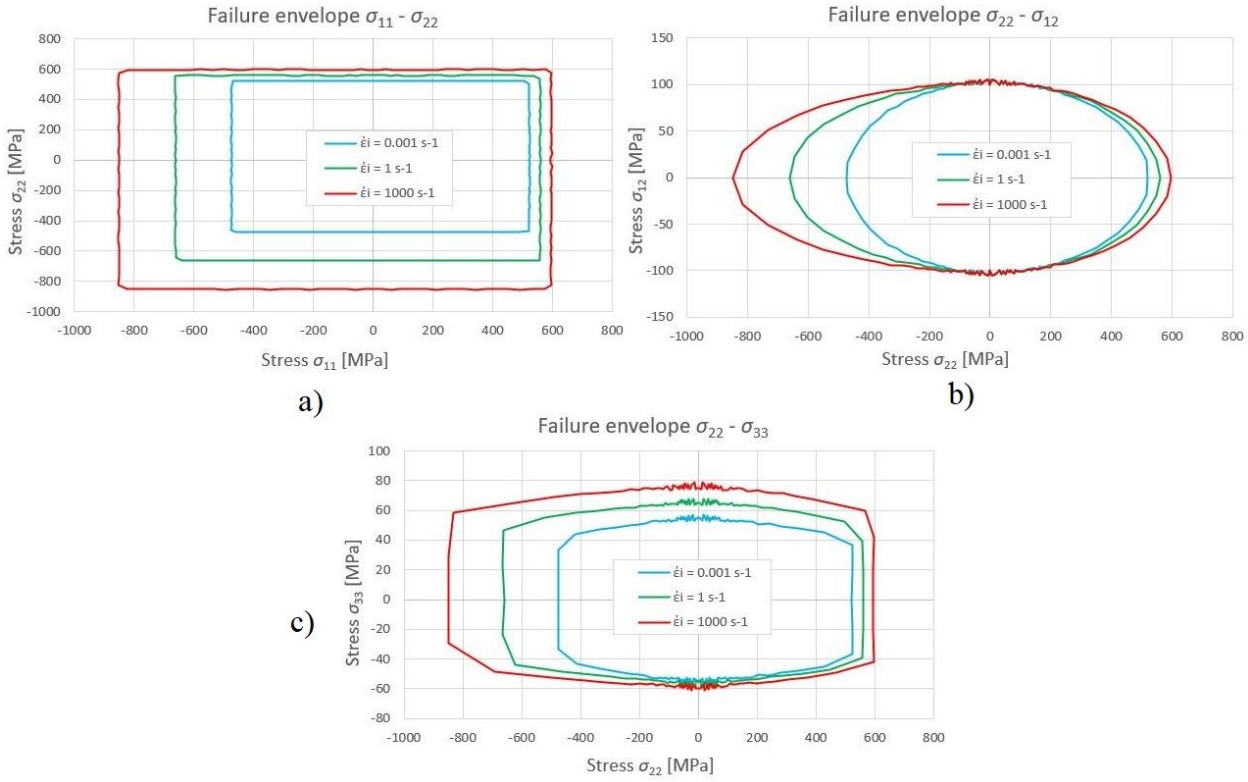

Figure 2: Failure envelopes for quasi-static (0.001 s^{-1}), intermediate (1 s^{-1}) and high (1000 s^{-1}) strain rates: a) in the $\sigma_{11} - \sigma_{22}$ plane, b) in the $\sigma_{22} - \sigma_{12}$ plane and c) in the $\sigma_{22} - \sigma_{33}$ plane

2.2. Failure initiation

The failure criteria applied in this study are based on the modified version of Hashin's failure theory proposed in [6], which distinguishes between eight different failure modes: warp and weft fiber direction tensile and compressive criteria, three shear failure criteria and a single matrix failure initiation criterion. These failure criteria are defined as

$$FF1T = \left(\frac{\sigma_{11}}{X_t^d}\right)^2 + \left(\frac{\tau_{12}}{S_{12}}\right)^2 + \left(\frac{\tau_{13}}{S_{13}}\right)^2 \geq 1, \tag{2}$$

$$FF1C = \left(\frac{\sigma_{11}}{X_c^d}\right)^2 + \left(\frac{\tau_{12}}{S_{12}}\right)^2 + \left(\frac{\tau_{13}}{S_{13}}\right)^2 \geq 1, \tag{3}$$

$$FF2T = \left(\frac{\sigma_{22}}{Y_t^d}\right)^2 + \left(\frac{\tau_{12}}{S_{23}}\right)^2 + \left(\frac{\tau_{23}}{S_{23}}\right)^2 \geq 1, \tag{4}$$

$$FF2C = \left(\frac{\sigma_{22}}{Y_c^d}\right)^2 + \left(\frac{\tau_{12}}{S_{23}}\right)^2 + \left(\frac{\tau_{23}}{S_{23}}\right)^2 \geq 1, \tag{5}$$

$$FS12 = \left(\frac{\tau_{12}}{S_{12}}\right)^2 \geq 0.999, \tag{6}$$

$$FS23 = \left(\frac{\tau_{23}}{S_{23}}\right)^2 \geq 0.999, \tag{7}$$

$$FS13 = \left(\frac{\tau_{13}}{S_{13}}\right)^2 \geq 0.999, \tag{8}$$

$$\begin{aligned} MFT = MFC = &\left(\frac{\sigma_{11}}{2 \cdot X_{t/c}^d}\right)^2 + \left(\frac{\sigma_{22}}{2 \cdot Y_{t/c}^d}\right)^2 + \left(\frac{\tau_{12}}{S_{12}}\right)^2 + \left(\frac{\tau_{23}}{S_{23}}\right)^2 \\ &+ \left(\frac{\tau_{13}}{S_{13}}\right)^2 + \left(\frac{\sigma_{33}^2}{Z_t^d \cdot Z_c^d}\right) + |\sigma_{33}| \cdot \left(\frac{1}{Z_{t,c}^d}\right) \geq 1. \end{aligned} \tag{9}$$

In eqs. (6) - (8), the shear stress components represent nonlinear shear stresses that are elaborated in detail in Section 2.3. The expressions used imply that failure is considered to have taken place when the left side of the equation reaches a value of 0.999, rather than 1. This distinction arises from the exponential non-linear formulation of the shear stresses based on shear strength values. This formulation ensures that shear stresses approach the material's strengths asymptotically, preventing them from surpassing those strengths.

A single matrix failure criterion, defined in eq. (9), is proposed in [5]. The last component of the summation sequence in this equation depends on the tensile or compressive character of σ_{33}. Consequently, $Z_{t,c}^d$ is equal to Z_t^d if σ_{33} is tensile and equal to Z_c^d if σ_{33} is compressive. Hence, if the σ_{33} is tensile, the value calculated by eq. (9) corresponds to matrix tensile failure indication (*MFT*), otherwise the value calculated by the same relation corresponds to matrix compressive failure indication (*MFC*). In this study, the matrix failure mode is currently implemented only as a failure initiation criterion, since the implementation of a damage model for this failure mode requires further investigation.

2.3. Non-linear shear response

As previously mentioned, non-linearity is especially pronounced in the shear response of the woven plies. The non-linear shear components are calculated by the relation [5]

$$\tau_{ij} = S_{ij} \cdot \left[1 - e^{\left(-\frac{G_{ij}^0 \cdot \gamma_{ij}}{S_{ij}}\right)}\right], \qquad i,j = 1,2,3, i \neq j, \tag{10}$$

where S_{ij} is the shear strength, G_{ij}^0 is the shear modulus and γ_{ij} is the instantaneous engineering shear strain. A shear stress obtained by the formulation presented in eq. (10) in the case of $S_{ij} = 100$ MPa and $G_{ij}^0 = 4$ GPa is depicted in Figure 3.

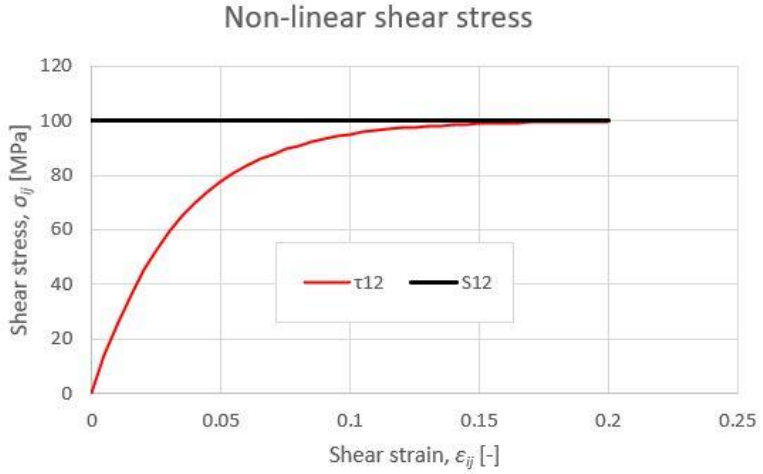

Figure 3. Non-linear shear stress - strain relationship

Furthermore, in order to utilize the progressive damage evolution, the shear strain is divided to elastic γ_{ij}^{el} and inelastic γ_{ij}^{in} components using the relation

$$\gamma_{ij}^{in} = \gamma_{ij} - \gamma_{ij}^{el}, \qquad i,j = 1,2,3, i \neq j, \tag{11}$$

where elastic component is simply obtained by

$$\gamma_{ij}^{el} = \frac{\tau_{ij}}{G_{ij}^0}, \qquad i,j = 1,2,3, i \neq j. \tag{12}$$

In eq. (12) τ_{ij} and G_{ij}^0 are the corresponding non-linear shear stress and shear modulus, respectively. While coding the VUMAT subroutine, it is essential to pay attention to changes from tensorial to engineering shear strain components during different calculation procedures and operations.

2.4. Damage propagation

Once the failure is initiated, a progressive damage model is induced according to linear degradation of nominal stress vector in the well-known manner

$$\sigma = (1 - d) \cdot \sigma', \tag{13}$$

where σ' is the nominal (undamaged) stress vector calculated from presumed orthotropic linear elastic behavior according to Hooke's law from stiffness matrix $\mathbf{C}$ and strain vector ε

$$\sigma' = \mathbf{C}\varepsilon. \tag{14}$$

The parameter d in eq. (13) is the damage variable vector that consists of damage variables defined in a way to degrade the corresponding stress components according to their appearance in the distinguished failure initiation criteria given above. For direct failure modes, based on the corresponding direct stress ii sign (+/-), the damage variable corresponding to tensile (superscript *t*) or compressive (superscript *t*) failure mode is calculated according to [6, 7] as

$$d_{ii}^{t/c} = \frac{\varepsilon_{ii}^{f} \cdot (\varepsilon_{ii} - \varepsilon_{ii}^{0})}{\varepsilon_{ii} \cdot \left(\varepsilon_{ii}^{f} - \varepsilon_{ii}^{0}\right)}, \tag{15}$$

where ε_{ii}^{0} is the strain at the onset of damage, ε_{ii} is the current strain, while ε_{ii}^{f} is the ultimate failure strain calculated as

$$\varepsilon_{ii}^{f} = \frac{2 \cdot \Gamma_i}{X_{ii} \cdot L_c}. \tag{16}$$

In eq. (16), Γ_{ii} is the critical strain energy release rate of mode ii, X_{ii} is the stress at onset of failure, i.e. strength of the material in the corresponding ii direction, i.e. failure mode, and L_c is the characteristic finite element length, introduced in order to avoid mesh-size dependency of the solution, as previously proposed in [5, 7] and many other references.

In the case of shear progressive damage, the damage variable is calculated in each step by the relation

$$d_{ij} = \frac{\gamma_{ij}^{f} \cdot \left[2 \cdot \left(\gamma_{ij} - \gamma_{ij,0}^{in}\right) - \gamma_{ij}^{f}\right]}{\left(\gamma_{ij}^{f} + \gamma_{ij,0}^{in} - \gamma_{ij}\right)\left(\gamma_{ij} - \gamma_{ij,0}^{in}\right)}, \tag{17}$$

as proposed firstly in [8], leading to linear material degradation. In eq. (17) γ_{ij}^{f} is the failure strain calculated by eq. (16), $\gamma_{ij,0}^{in}$ is the inelastic component of the shear strain at failure initiation, and γ_{ij} is the instantaneous shear strain.

Based on the detailed explanation given above, the model distinguishes between seven different damage variables in total. Finally, knowing the form of failure initiation criteria given by eqs. (2) - (9), the stress component degradation relations given firstly by eq. (13) can be expanded as

$$\begin{bmatrix}\sigma_{11}\\ \sigma_{22}\\ \sigma_{33}\\ \sigma_{12}\\ \sigma_{23}\\ \sigma_{13}\end{bmatrix} = \begin{bmatrix} (1-d_{11}^{t}) \cdot (1-d_{11}^{c}) \\ (1-d_{22}^{t}) \cdot (1-d_{22}^{c}) \\ 1 \\ (1-d_{11}^{t})(1-d_{11}^{c}) \cdot (1-d_{22}^{t})(1-d_{22}^{c}) \cdot (1-d_{12}) \\ (1-d_{22}^{t}) \cdot (1-d_{22}^{c}) \cdot (1-d_{23}) \\ (1-d_{11}^{t}) \cdot (1-d_{11}^{c}) \cdot (1-d_{13}) \end{bmatrix}^{T} \cdot \begin{bmatrix}\sigma'_{11}\\ \sigma'_{22}\\ \sigma'_{33}\\ \sigma'_{12}\\ \sigma'_{23}\\ \sigma'_{13}\end{bmatrix}. \tag{18}$$

Finite element deletion is ordered in the specific cases when damage variables corresponding to fiber damage (either tensile or compressive) in both fiber directions have reached their full values that were set to 0.99. No element deletion is related to shear material failure in the current model.

2.5. Numerical model

The numerical impact simulations in this work replicate the experimental conditions in [5,7]. In these experiments, a 23.8 mm diameter steel spherical impactor of 54.7 g mass impacts a cantilever fixtured square CFRP panel of 195 x 195 mm^2 surface area at various initial velocities. The nominal plate thickness is 5.58 mm, consisting of a total of 10 plies with two outer (surface) plies of thickness of 0.31 mm and eight mid (bulking) plies of a nominal thickness of 0.62 mm. All plies were placed in the same orientation ([0°, 90°]), thus contributing to the assumption of orthotropic laminate behavior. The applied mechanical properties of the woven CFRP material are presented in Table 2, after [5].

Table 2. Properties of T300 K3/IMP530R and T300 K12/IMP530R material system [5]

Property	Unit	Value
$E_1 = E_2$	[GPa]	51.000
E_3	[GPa]	8.000
G_{12}	[GPa]	4.032
$G_{23} = G_{13}$	[GPa]	3.000
ν_{12}	[-]	0.060
$\nu_{23} = \nu_{13}$	[-]	0.300
$\Gamma_{11t} = \Gamma_{22t}$	[kJ/m^2]	75.000
$\Gamma_{11c} = \Gamma_{22c}$	[kJ/m^2]	25.000
Γ_s	[kJ/m^2]	2.250

The numerical model with boundary and initial conditions, along with the mesh visualization, is depicted in Figure 4. In this work, two impact cases were simulated. These cases differ in the initial impactor velocity. The velocity in the first case is 59.5 m/s, whereas the initial velocity in the second case is 78.5 m/s. These initial velocities correspond to the initial kinetic energies of 96.8 J and 168.5 J, respectively.

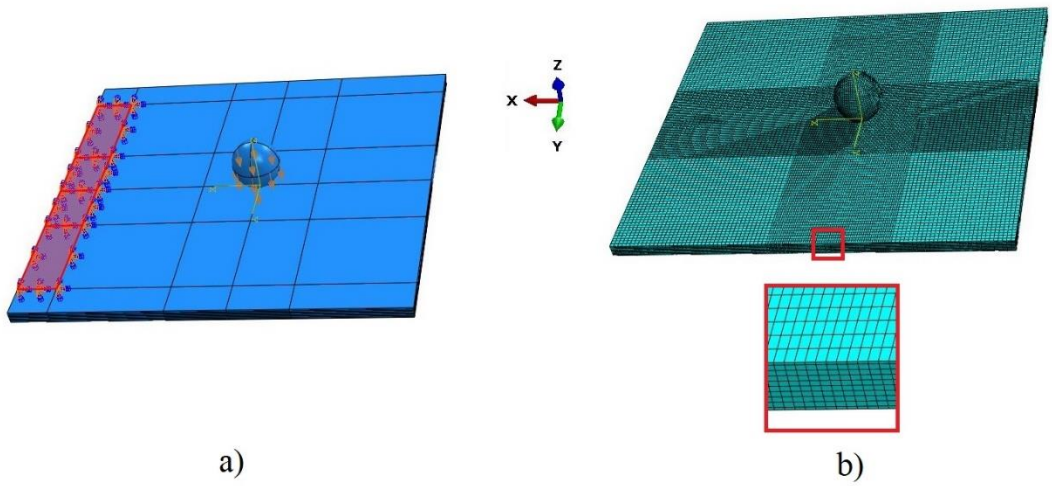

Figure 4: Numerical model: a) prescribed boundary and initial conditions, b) mesh discretization with a detailed view of the through-thickness discretization

The composite plate is discretized using 163840 first order hexagonal finite elements with reduced integration (C3D8R). One finite element through the thickness of each ply was employed. Varying size of finite elements was used for the sake of computational efficiency. Therefore, an approximate size of 1 mm of an element is used at the impact location, while an

average size of 2 mm is utilized to discretize the model further from the impact location.

The steel impactor is discretized using a total number of 12744 C3D8R elements. The impactor is modelled as a linearly elastic deformable body with mechanical properties provided in [5].

Table 3. Steel impactor material properties

Property	Unit	Value
E	[GPa]	210
ν	[-]	0.3
ρ	[kg/m^3]	7750

3. RESULTS

The time history of the displacement field during the impact for the 59.5 m/s initial velocity is shown in Figure 5. Figure 6 illustrates the comparison of out-of-plane displacements along vertical and horizontal paths across the plate measured from the initial impact location for the lower impactor velocity (59.5 m/s). Similarly, Figure 7 displays this comparison for the higher initial impactor velocity (78.5 m/s). These results are shown at selected time intervals to enable comparison with experimental results published in [5, 7].

As shown in Figure 6 and Figure 7, the obtained numerical results correlate reasonably well with the experimentally obtained results from [5, 7]. Somewhat larger discrepancies can be observed from the results in Figure 7 where the results for the higher impact velocity are shown. Some of the differences between numerical and experimental results in Figures 6 and 7 might originate simply from the initial distance of the impactor to the plate in the numerical model and the resulting difference in the time sequences.

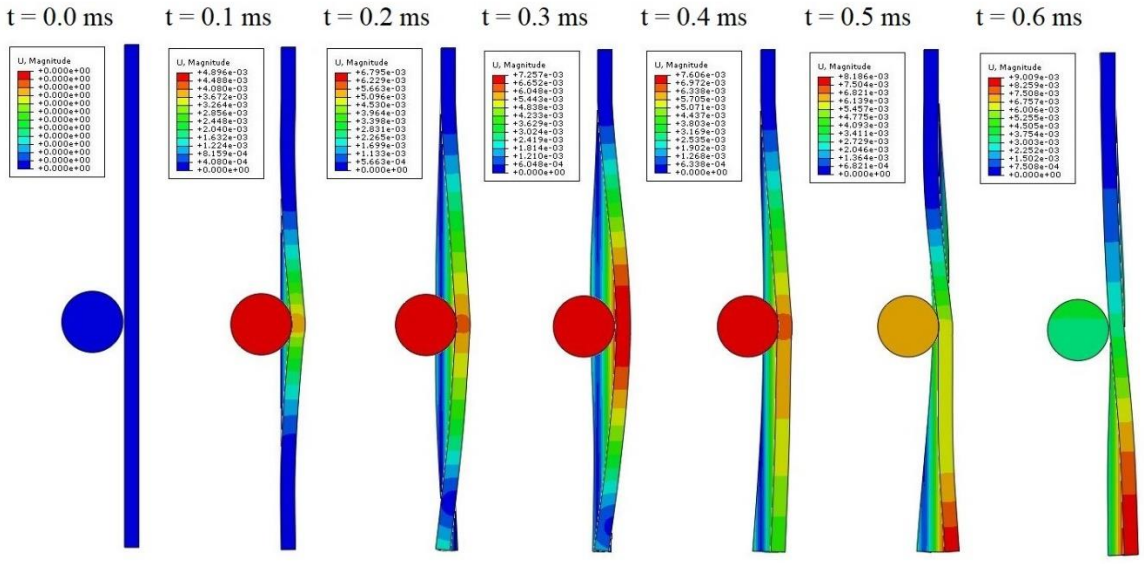

Figure 5. Time history of the impact event at 59.5 m/s with displacement [m] fields shown

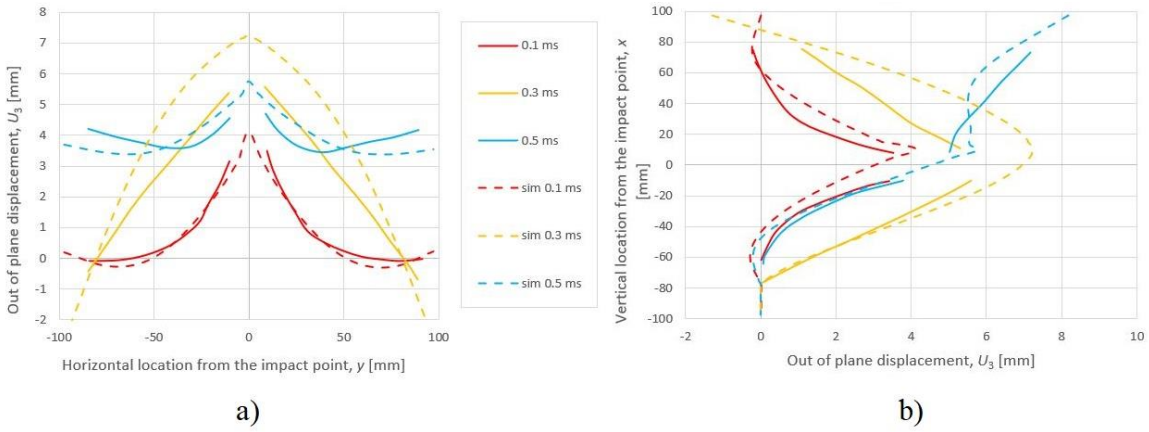

Figure 6. Out-of-plane displacement fields at the 59.5 m/s impact: a) over horizontal path, b) over vertical path

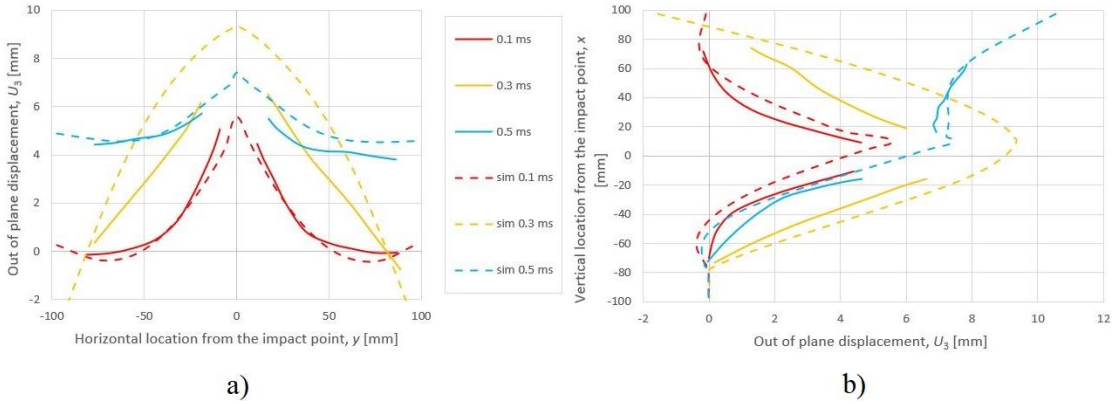

Figure 7: Out-of-plane displacement fields at the 78.5 m/s impact: a) over horizontal path, b) over vertical path

Fiber damage parameters for tensile and compressive damage in both in-plane directions for the 59.5 m/s impact are presented in Figure 8. As it was previously mentioned, the maximum damage parameter value is set to 0.99 due to numerical calculation procedure reasons.

As depicted in Figure 8, tensile fiber damage occurs in both in-plane directions primarily in the lower part of the plate, gradually expanding toward the plate's backface. On the other hand, compressive damage is localized on the impacted plate face, which aligns with expectations for convex contact scenarios. The distributions of damage parameters shown in Figure 8 contribute to verifying the developed constitutive model's validity, leading to the conclusion that the developed progressive damage model provides physically accurate solutions.

4. DISCUSSION

A source of discrepancies that might have significant impact on the results is the lack of the of strain rate effects on the material elasticity properties. Also, an interesting strain rate-dependent damage propagation model designated specifically for plain woven composites is proposed in [9] and is planned to be tested in the future with the here examined failure initiation model.

As previously mentioned, in the current model no damage propagation is implemented following the matrix damage initiation due to the lack of adequate matrix failure theories for woven composites. The finite element deletion strategy employed in this work, presenting total

material point failure only when the fibers have failed in both in-plane directions has been selected based on the trial-and-error method. This approach will also be validated in the future research. Finally, an important further research phase is the implementation of an interply damage model that would enable modelling of delaminations. Further development of the presented model is planned by implementation of the delamination model introduced in [10].

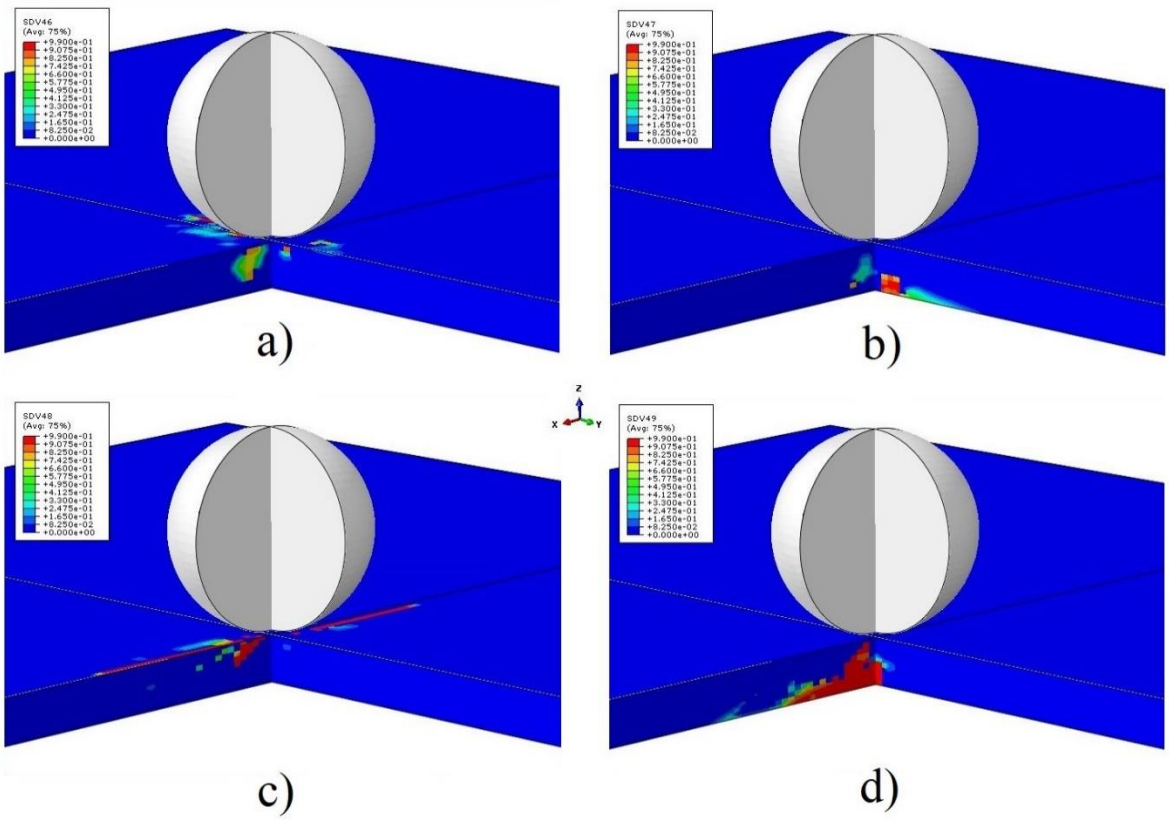

Figure 8: Fiber damage parameter distribution for the 59.5 m/s impact: a) d_{f11c}, b) d_{f11t}, c) d_{f22c}, d) d_{f22t}

5. CONCLUSIONS

This study presents an overview of the current state of ongoing research, focusing on the development of a strain rate-dependent constitutive model for woven CFRP composites. This model consists of a failure initiation theory that considers strain rate effects, along with the implementation of progressive damage model. The model was applied for simulation of impact in laminated CFRP plates at high velocities, leading to reasonably accurate results.

Future development plans include a more detailed consideration of the integration of strain-rate effects for woven composites. This includes investigation of the potential correlation between elevated stiffness parameters and, potentially, fracture toughness with increasing strain rates. Moreover, enhancing the fidelity of damage evolution laws and implementing more accurate failure initiation criteria could potentially enhance the predictive accuracy of impact damage in woven composite structures. Furthermore, the introduction of delamination failure mode in the model is seen from the perspective of the authors as holding significant promise for generating more precise simulation results and thus achieving more reliable results.

ACKNOWLEDGEMENTS

The research is fully funded by the Croatian Science Foundation (HRZZ) within the project

"Computational Modelling of Composite Structures Impact Damage" (CONCORDE), grant number UIP-HRZZ-2020-02-9317.

REFERENCES

[1] H. Koerber and P.P. Camanho, High strain rate characterization of unidirectional carbon epoxy IM7-8552 in longitudinal compression, *Composites: Part A*; Vol. 42(5), 2011, pp. 462-470, (doi: 10.1016/j.compositesa.2011.01.002).

[2] M. H. Kashani and A. S. Milani, Damage Prediction in Woven and Non-woven Fabric Composites, In *Non-woven Fabrics*, InTechOpen: Rijeka, Croatia, 2016, pp. 223–262.

[3] I. K. Giannopoulos, M. Yasaee, and N. Maropakis, Ballistic Impact and Virtual Testing of Woven FRP Laminates, *Journal of Composites Science*, Vol. 5(5), 2021, pp. 115-129, (doi: 10.3390/jcs5050115).

[4] F. Martinez-Hergueta, D. Ares, A. Ridruejo et al., Modelling the in-plane strain rate dependent behaviour of woven composites with special emphasis on the non-linear shear response, *Composite Structures*, Vol. 210, 2018, pp. 840-857, (doi: 10.1016/j.compstruct.2018.12.002).

[5] L. A. Coles, A. Roy, and V. Silberschmidt, Ice Vs. Steel: Ballistic Impact of Woven Carbon/epoxy Composites. Part II – Numerical Modelling, *Engineering Fracture Mechanics*, Vol. 225, 2019, pp. 106297-106314, (doi: 10.1016/j.engfracmech.2018.12.030).

[6] L. Raimondo, L. Iannucci, P. Robinson and P.T. Curtis, Modelling of strain rate effects on matrix dominated elastic and failure properties of unidirectional fibre-reinforced polymer-matrix composites, *Composite Science and Technology*, Vol. 72, 2012, pp. 819-827, (doi: 10.1016/j.compscitech.2012.02.011).

[7] L. A. Coles, A. Roy, N. Sazhenkov et al., Ice Vs. Steel: Ballistic Impact of Woven Carbon/epoxy Composites. Part I – Deformation and damage behaviour, *Engineering Fracture Mechanics*, Vol. 225, 2019, pp. 106270-106287, (doi: 10.1016/j.engfracmech.2018.12.003).

[8] Y. Shi, T. Swait, C. Soutis: Modelling damage evolution in composite laminates subjected to low velocity impact, *Composite Structures*, Vol 94, 2012, pp. 2902-2913, (doi: 10.1016/j.compstruct.2012.03.039).

[9] X. Hu, J. Tang, W. Xiao and K. Qu, A Strain Rate Dependent Progressive Damage Model for Carbon Fiber Woven Composites under Low Velocity Impact, *2021 The 2nd International Conference on Mechanical Engineering and Materials (ICMEM 2021) 19-20 November 2021, Beijing, China*, Journal of Physics: Conference Series, 2021, Vol. 2101, pp. 012073-012079, (doi: 0.1088/1742-6596/2101/1/012073).

[10] Z. Liu, Y. Xia, and S. Guo, Characterization methods of delamination in a plain woven CFRP composite, *Journal of Material Science*, Vol. 54, 2019, pp. 13157–13174, (doi: 10.1007/s10853-019-03847-4).